AIAA Paper No. 97-3778

Robust, Decoupled, Flight Control Design With Rate Saturating Actuators

S. A. Snell[1] and R. A. Hess[2]
Dept. of Mechanical and Aeronautical Engineering
University of California
Davis, CA 95616

Abstract

Techniques for the design of control systems for manually controlled, high-performance aircraft must provide the following: (1) multi-input, multi-output (MIMO) solutions, (2) acceptable handling qualities including no tendencies for pilot-induced oscillations, (3) a tractable approach for compensator design, (4) performance and stability robustness in the presence of significant plant uncertainty, and (5) performance and stability robustness in the presence actuator saturation (particularly rate saturation). A design technique built upon Quantitative Feedback Theory is offered as a candidate methodology which can provide flight control systems meeting these requirements, and do so over a considerable part of the flight envelope. An example utilizing a simplified model of a supermaneuverable fighter aircraft demonstrates the proposed design methodology.

Introduction

The flight control system design technique to be described is an outgrowth of several recent research efforts.[1-5] The work has been motivated by the realization that a significant number of high-performance aircraft, particularly those with fly-by-wire flight control systems, have experienced shortcomings in control and handling qualities in developmental flight test.[6] These problems, some of which have been quite severe, can often be attributable to a failure of the control system design technique to provide (1) multi-input, multi-output (MIMO) solutions, (2) acceptable handling qualities including no tendencies for pilot-induced oscillations, (3) a tractable approach for compensator design, (4) performance and stability robustness in the presence of significant plant uncertainty, and (5) performance and stability robustness in the presence actuator saturation (particularly rate saturation).

In the following, a methodology is presented for meeting the requirements just stated. For the sake of clarity, the methodology will be couched in terms of a specific flight control example. The example presents a challenging problem, and the vehicle model is readily available for the interested reader. A description of the example problem begins the presentation. This is followed by a discussion of the Quantitative Feedback Theory (QFT) procedure, with particular emphasis upon the direct determination of an approximately diagonalizing precompensator and the use of a Pre-Design Technique (PDT) which offers considerable insight into the formal QFT design. A procedure for improving the performance of the QFT design in the presence of actuator rate saturation follows. The results of the QFT design are then presented including a nonlinear simulation in which actuator amplitude and rate saturation are considered. A statement of conclusions closes the discussion.

The Flight Control Example

System Structure

Figure 1 is a block diagram representation of the flight control design to be discussed: the determination of a stability and command augmentation system for the lateral-directional control of a high-performance aircraft. The vehicle in question is represented by a simplified model of a supermaneuverable fighter aircraft whose linearized dynamics are given in Ref. 7, and which, in one form or another, has been used in a variety of related studies.[2,8,9] Fifteen flight conditions are to be considered in the design, ranging from Mach No. = 0.3 and altitude = 10,000 ft, to Mach No. = 0.9 and altitude = 30,000 ft.

[1]Assistant Professor, Senior Member AIAA.

[2]Professor, Associate Fellow AIAA.

Starting from the far right in Fig. 1, the vehicle is presented by the matrix of plant transfer functions $P(s)$. The vehicle response variables to be controlled are body-axis roll rate $p(t)$, and sideslip angle $\beta(t)$. An inner feedback loop involving feedback of washed-out yaw rate $r(t)$ is employed to improve dutch-roll damping across the 15 flight conditions. As shown in Fig. 1, the vehicle possesses five lateral-directional control effectors: differential horizontal tail δ_{DT}, aileron δ_A, rudder δ_R, differential pitch thrust vectoring δ_{RTV}, and yaw thrust vectoring δ_{YTV}. The matrix K is a 5x2 *control distribution matrix*, each row of which contains only a single non-zero entry. For reasons discussed in Ref. 2, this non-zero entry is set equal to the *rate limit* (deg/s) of the particular (and only) control surface actuator which it effects. Selection of the control effectors to associate with each output variables was made on the basis of the control effectiveness of each device.

The control distribution matrix allows the use of "software" rate limiters, each of which is defined by three elements (differentiator, limiter, and integrator) providing inputs $u_1(t)$ and $u_2(t)$ to K. It's important to point out that the differentiators "s" in Fig. 1 are always subsumed into the compensators which precede them, e.g., the elements of the matrix compensator $G_{c_p}(s)$ and the single element $G_r(s)$.

Performance and Stability Specifications

The control system performance specifications are stated as performance and stability bounds. The performance bounds relate to the magnitudes of the following transfer functions evident in Fig. 1: $\left|\frac{\beta}{\beta_c}(j\omega)\right|$, $\left|\frac{p}{p_c}(j\omega)\right|$, $\left|\frac{\beta}{p_c}(j\omega)\right|$, $\left|\frac{p}{\beta_c}(j\omega)\right|$. The first two of these functions define *tracking bounds*, while the latter two define *cross-coupling bounds*. For the tracking bounds, both upper and lower limits are prescribed, while for the cross-coupling bounds, only upper magnitude are needed. In addition to the performance bounds just described, stability bounds are also defined. These may be handled in a number of ways, but here will be specified as maximum amplitude ratios on the closed-loop transfer functions defining tracking behavior.

In this example, attention will be focused upon roll attitude as the variable of interest to the pilot in manual, closed-loop tracking. Sideslip will not be considered as a tracking variable, although specifications will still be placed upon input-output and cross-coupling relations as just described. The pilot modeling procedure described in Ref. 3 will be used to prescribe the roll-rate tracking bounds $\left|\frac{p}{p_c}(j\omega)\right|$ so as to yield predicted level 1 handling qualities (assuming a roll-attitude loop is closed by the pilot) and no predicted susceptibility to pilot-induced oscillations across the 15 flight conditions.

The QFT Procedure

Diagonal Compensation

The application of QFT to flight control problems has been described rather extensively in the literature, e.g., Ref. 10. No detailed discussion of the QFT design philosophy will be presented herein. However, one element of the QFT procedure will be discussed, i.e., the use of diagonal compensation. As typically applied, the QFT design procedure involves input-output pairing. This means associating one or more control effectors exclusively with the control of an output or response variable. With this accomplished, one is left with a diagonal compensation matrix, and the so-called "Method 1" (original) or "Method 2" (improved) QFT design techniques are followed.[11] Either of these approaches places the burden of providing desired tracking and cross-coupling performance on the elements of the diagonal compensation matrix. It is obvious that some reduction in conservatism can be gained by a design procedure which employs a non-diagonal compensation matrix. A number of such approaches have been suggested for achieving non-diagonal compensation,[12,13,14] all of which create a precompensation matrix (shown in Fig. 1 as $G_{c_p}(s)$). For the QFT design, this precompensation matrix is considered part of the plant matrix (now referred to as the effective plant matrix $P_e(s)$) and a diagonal QFT compensation matrix is then designed (shown in Fig. 1 as $G_c(s)$). The QFT diagonal compensation matrix then postmultiplies the precompensation matrix to form a final, non-diagonal compensation matrix $G_{c_p}(s)\cdot G_c(s)$ to be implemented in the flight control computer.

A problem which can occur with previous methods for achieving non-diagonal compensation is that it may be quite difficult to design the diagonal QFT compensator given the effective plant formed by

postmultiplying the original plant by the precompensation matrix. This problem can be overcome by the procedure outlined next.

Precompensation using Dynamic Inversion

Introduction Dynamic inversion is a well-known technique for controlling nonlinear systems.[15] Consider the square, linear, time-invariant system, with an *nx1* state vector $\boldsymbol{x(t)}$, an *mx1* input vector $\boldsymbol{u(t)}$ and an *rx1* output vector $\boldsymbol{y(t)}$

$$\begin{aligned} \dot{\boldsymbol{x}} &= \boldsymbol{Ax}+\boldsymbol{Bu} \qquad (a) \\ \boldsymbol{y} &= \boldsymbol{Cx}+\boldsymbol{Du} \qquad (b) \end{aligned} \tag{1}$$

The inverse dynamics of the system of Eq. 1 can be obtained by differentiating the individual elements of $\boldsymbol{y(t)}$ a sufficient number of times until a term involving an element of the input $\boldsymbol{u(t)}$ appears. After d such differentiations, the output equation becomes

$$\boldsymbol{y^{[d]}} = \boldsymbol{A'x}+\boldsymbol{B'u} \tag{2}$$

where $\boldsymbol{[d]}$ is an rx1 vector containing the order of differentiation of each element of $\boldsymbol{y(t)}$. A sufficient condition for the existence of an inverse system to Eq. 1 is that $\boldsymbol{B'}$ in Eq. 2 have rank r. If this is the case, the inverse system model takes the form of a state variable feedback controller as

$$\begin{aligned} \dot{\boldsymbol{x}} &= [\boldsymbol{A}-\boldsymbol{B}(\boldsymbol{B'})^{-1}\boldsymbol{A'}]\boldsymbol{x}+\boldsymbol{B}(\boldsymbol{B'})^{-1}\boldsymbol{v} \qquad (a) \\ \boldsymbol{u} &= -(\boldsymbol{B'})^{-1}\boldsymbol{A'x}+(\boldsymbol{B'})^{-1}\boldsymbol{v} \qquad (b) \end{aligned} \tag{3}$$

where $(\boldsymbol{B'})^{-1}$ is a right pseudo-inverse of $\boldsymbol{B'}$ and where

$$\boldsymbol{v} = \boldsymbol{y^{[d]}} \tag{4}$$

Equations 3 and 4 have created an integrator-decoupled system, i.e., the controls are decoupled and the dynamics appear as pure integrators with v as an input vector. Desirable linear dynamics between each output y_i and new external inputs w_i, are given by setting

$$v_i = -\sum_{k=1}^{d_i-1} a_{i,k}y_i^{[k]}+a_{i,0}w_i \qquad i=1,2,...m \tag{5}$$

or

$$\boldsymbol{v} = \boldsymbol{C'x}+\boldsymbol{D'w} \tag{6}$$

decoupled dynamics are created as

$$y_i^{[d_i]}+a_{i,d_i-1}y_i^{[d_i-1]}+\cdots+a_{i,0}y_i = a_{i,0}w_i \tag{7}$$

If $\sum_{i=1}^{m} d_i = p$ then p poles of the original plant can be placed. Since the system being controlled is assumed linear, no actual state feedback is required to create the dynamic inverse. Rather a precompensation matrix is defined from Eqs. 3 and 5 which relates w and u, the input and output of the linear model/dynamic inverse system, respectively. The well-known inability of dynamic inverse designs to handle non-minimum phase systems can be surmounted by forming a "regulated variable" which is minimum phase[16] or possibly through the feedback of independent, internal variables. As will be seen, yaw rate r was served as an internal variable in the present application.

Application to Uncertain Systems Dynamic inversion is an excellent candidate for forming a precompensation matrix for QFT. This is because it can approximately decouple a system, while creating an effective plant which is easily compensated using the Nichols chart, the primary graphical tool for QFT design. However, since it is desired to minimize gain scheduling, a *single* dynamic inverse must be chosen for the set of flight conditions which define the plant uncertainty. One way to accomplish this is to consider the set of precompensation matrices $\boldsymbol{G_{c_p}(s)}$ for all the flight conditions, then create the elements of a single such matrix which, in the complex plane, minimizes the maximum deviation between itself and all other corresponding elements in the set. This minimization is carried out over the frequency range of interest. However, in practice, this procedure is usually unnecessary as the $\boldsymbol{G_{c_p}(s)}$ associated with one of the configurations being analyzed can usually be selected which approximately meets the criterion just described.

Feedback of Internal Variables The use of a single dynamic inverse to approximately decouple the plant and to provide simplified effective dynamics for eventual compensation in the formal QFT procedure can often be expedited by the feedback of one or more independent "internal" variables prior to calculating any dynamic inverse. Independent internal variables refer

to variables other than the response or output variables (or their derivatives). In applications such as flight control, the feedback of internal variables can increase the damping of oscillatory modes, and as such, can improve the ability of a single dynamic inverse to effectively decouple the plant across the range of configurations being considered in the design. In addition, feedback of these internal variables can reduce uncertainty and possibly eliminate any non-minimum phase dynamics which may exist in the plant matrix $P(s)$.

A QFT Pre-Design Technique

As the name implies QFT design is *quantitative*. It requires quantitative specification of desired performance and uncertainty. As described in the preceding, employing QFT in the frequency domain requires the designer to specify bounds on the amplitude ratios of "on-axis" and "off-axis" response-to-command transfer functions (desired tracking performance and desired cross-coupling minimization). While specifying tracking bounds is fairly straightforward, especially in flight control problems where handling qualities specifications can provide some guidance, the specification of cross-coupling bounds can be problematic. This is not a minor concern as these cross-coupling bounds can drive the entire QFT design. Finally, multi-input, multi-output (MIMO) QFT designs are usually approached using a sequential loop closure technique to minimize conservatism.[11] Until now, no method other than trial and error could be employed to determine the loop closure sequence. As will be seen, both the problem of determining cross-coupling bounds and loop closure sequence can be solved using an approximate "Pre-Design Technique" (PDT). The details of this technique can be found elsewhere,[5] however a brief discussion is in order, herein.

The Pre-Design Technique has its basis in an assumption regarding the diagonal compensation elements of $G_c(s)$. Referring to the example, if the "pseudo-controls" w_1 and w_2 are approximately decoupled, then the following relationships can be employed

$$G_{c_{\beta\beta}} \approx \frac{\omega_{c_\beta}}{s}\cdot\frac{1}{(\beta/w_1)}; \qquad G_{c_{pp}} \approx \frac{\omega_{c_p}}{s}\cdot\frac{1}{(p/w_2)} \quad (8)$$

where the double subscripts on the left hand sides of the equations represent diagonal elements, the $\omega_{c_{(\cdot)}}$ represent crossover frequencies and the β/w_1 and p/w_2 represent the diagonal elements of $P_e(s)$. For the sake of simplicity, no actuator dynamics are included in determining $P_e(s)$ for the PDT design. Equation 8 exploits the well-known fact that the loop transmission $L(s)$ of a well-designed single-input, single-output (SISO) system, or the loop transmissions of an approximately decoupled MIMO system, each resemble $\omega_{c_{(\cdot)}}/s$ near the region of crossover. Equation 8 extends this approximation to all frequencies. In terms of approximating the elements of $G_c(s)$, low frequency characteristics ($\omega << \omega_c$) are relatively unimportant provided $|L(j\omega)| >> 1.0$, and high frequency characteristics ($\omega >> \omega_c$) are relatively unimportant provided $|L(j\omega)| << 1.0$. These conditions are guaranteed by Eq. 8. Note that stability is assumed in the PDT. For QFT designs, a nominal plant is selected to define a nominal loop transmission on the Nichols chart. For the PDT, this simply means choosing one of the possible plants out of the uncertain set to define the denominator of the right hand sides of Eq. 8. With the approximations of Eq. 8, approximate closed-loop transfer functions $(I+P_eG_c)^{-1}P_eG_cF$ can be obtained. The PDT will thus yield estimates of tracking and cross-coupling performance, and crossover frequencies can be made. These computations can be done very quickly on a personal computer, using readily available computer-aided-design software.

Improving Performance in the Presence of Actuator Rate Saturation

It has been demonstrated for a class of control systems that the use of "software rate limiters" can offer significant improvement in command-following performance when control actuators undergo rate saturation.[2] A pair of such software limiters are shown in Fig. 1. In Ref. 2, the use of such limiters was restricted to a class of systems in which each actuator could receive its input from only one compensated error signal. As demonstrated in Ref. 2, the software limiters improve performance by ensuring that each actuator never receives an input rate exceeding the limits of the device. In addition, the software limiters come out of saturation as soon as their input rates become smaller than the limiting values. This behavior is in contrast to that of a typical actuator undergoing rate saturation where the device remains in saturation until the actuator output (a displacement) equals its commanded input. This latter behavior introduces an

effective time delay in the control system, often with dire consequences.[6,17]

An analytical approach to describing the action of the software limiters can be made by again considering Fig. 1, where now the software limiters have been replaced by injected remnant signals, $n_i(t)$. It is assumed that the limiters prevent rate saturation of the actuators, themselves, so that the software limiters are the only nonlinearities present in the system. Conceptually, each and every signal in the quasi-linear system can be forced to be identical to that in the nonlinear system for any command inputs by the injection of appropriate $n_i(t)$ (where the possibility of amplitude saturation is not considered). Now if one could select elements of the compensator matrix $G_{c_p}(s)$ such that these $n_i(t)$ have no effect upon the vehicle response variables, then system performance would be completely unaffected by the presence of the software rate limiters. This would occur since the software limiters are, by design, preventing saturation of the actuators, and the saturation which is occurring in the software devices (represented by the injected remnant) is having no effect upon system response. Of course, such a situation is not possible. However, the effect of the injected remnant can be reduced considerably in a frequency range below crossover. This is accomplished in a loop-shaping design by appropriately selecting the "type" of the elements in $G_c(s)$ where "type" refers to the exponent on any free s's in the compensator transfer function.

In the work of Ref. 2, for a flight control system similar to that of Fig. 1, explicit expressions were developed for transfer functions $\frac{E_\beta}{n_1}(s)$, $\frac{E_\beta}{n_2}(s)$, $\frac{E_p}{n_1}(s)$, $\frac{E_p}{n_2}(s)$. These expressions were used to develop specifications on the type of the compensators and loop transmissions. These analytical results were predicated on the aforementioned assumption of each actuator being driven by the output of one and only one compensated error signal. However, by considering $\left|\frac{\beta}{n_1}(j\omega)\right|$, $\left|\frac{\beta}{n_2}(j\omega)\right|$, $\left|\frac{p}{n_1}(j\omega)\right|$, $\left|\frac{p}{n_2}(j\omega)\right|$, and adjusting the type of the compensator elements to achieve a desired reduction in these magnitudes over a limited but important frequency range (below crossover), the assumption just stated can be obviated. That is, each actuator can be driven by more than one compensated error signal and the benefits of the software limiters can still be obtained. This is obviously a desirable result from the standpoint of flight control system design wherein control effectors often play multiple roles. As discussed in Ref. 2, a tradeoff exists in this approach, since increasing the type of the compensation elements improves tracking under actuator rate saturation, but reduces linear stability margins.

The Design

Handling Qualities

To begin the design, acceptable tracking bounds for the roll-rate tracking loop are established. Figure 2 shows the structural model of the human pilot which is used to make predictions about handling qualities level and PIO susceptibility. Using the procedure described in Ref. 3, the Handling Qualities Sensitivity Function (HQSF) is determined when candidate upper and lower tracking bounds are specified for $\left|\frac{p}{p_c}(j\omega)\right|$. In the pilot/vehicle analysis, each of these bounds are considered to describe the plant of a SISO system under manual control. Referring to Fig. 2, the HQSF is defined as $\left|\frac{U_M}{C}(j\omega)\right|$ and the structural model parameters are selected as described in Ref. 3. Figure 3 shows the areas which, if penetrated by the HQSF, indicate the predicted vehicle handling qualities level. Also shown in the figure are the HQSF's generated by the structural model for the upper and lower p-loop tracking bounds described in what follows.

Figure 4 shows boundaries associated with $\Phi_{u_m u_m}(\omega)$, the power spectral density of the signal U_M in the pilot model of Fig. 2. $\Phi_{u_m u_m}(\omega)$ is calculated with a specific input power spectral density as described in Ref. 3. In Fig. 4, the predicted pilot-induced oscillation rating (PIOR) is determined by the area penetrated by $\Phi_{u_m u_m}(\omega)$ when the structural model parameters are selected as described in Ref. 3. Also shown in Fig. 4 are the $\Phi_{u_m u_m}(\omega)$'s generated by the structural model for the upper and lower p-loop tracking bounds in Fig. 5. The rather small violation of the bound $2 < PIOR < 4$ was not considered significant, here. Obviously, tracking bounds selected in this manner are not unique. However, they are predicted to yield a level 1 (satisfactory) handling

qualities and a $1 \le PIOR \le 2$ (no tendency for pilot to induce undesirable motions).

Dynamic Inversion for the PDT

In attempting to find a single dynamic inverse for use across the 15 configurations which defined the plant uncertainty, it was found that the lightly-damped dutch-roll mode caused problems, as rather small changes in the dutch-roll frequency from configuration to configuration made it difficult for a single dynamic inverse to provide effective decoupling and simplified dynamics. However, by defining washed-out yaw-rate as an internal variable, and feeding this variable back as shown in Fig. 1, the situation was improved considerably. The feedback transfer function G_r in Fig. 1 was defined as

$$G_r = \frac{-3s}{s+1} \qquad (a)$$
$$or \qquad (9)$$
$$sG_r = \frac{-3s^2}{(s+1)(.01s+1)} \qquad (b)$$

where Eq. 9b was used when the software rate limiters were employed and the differentiating "s" in Fig. 1 was to be subsumed into $G_r(s)$ as described in the preceding. The output of $G_r(s)$ was fedback to the rudder and the yaw-thrust vectoring through the control distribution matrix, **K**, shown in Table 1. The washout was employed to allow the pilot to perform coordinated turns. The selection of washed-out yaw rate as an independent internal variable has been used in another flight control study for this vehicle.[9]

With no actuator dynamics included in the PDT application of the dynamic inverse technique led to a nominal effective plant matrix

$$\mathbf{P}_e(s) = \begin{bmatrix} \frac{1}{s} & 0 \\ 0 & \frac{1}{s} \end{bmatrix} \qquad (10)$$

The PDT

Figures 5 and 6 show $\left|\frac{\beta}{\beta_c}(j\omega)\right|$, $\left|\frac{p}{p_c}(j\omega)\right|$, $\left|\frac{\beta}{p_c}(j\omega)\right|$, $\left|\frac{p}{\beta_c}(j\omega)\right|$ which resulted from the PDT. The bounds on the roll-rate tracking were selected as described in the preceding. Also mentioned in the preceding, the bounds on $\left|\frac{\beta}{\beta_c}(j\omega)\right|$ were not based upon handling qualities or PIO susceptibility, as the β loop was not considered a tracking loop, *per se*. The bounds shown were considered to provide acceptable open-loop response to cockpit pedal inputs. The dashed curves in Fig. 6 represent cross-coupling bounds to be used in the formal QFT procedure. In generating the performance results shown in Figs. 5 and 6, the nominal flight condition was chosen as Mach No. = 0.6, altitude = 20,000 ft and The loop crossover frequencies defined for the nominal plant were ω_{c_β} = 3.0 *rad/s*, ω_{c_p} = 6.0 *rad/s*.. Prefilter transfer functions $F_\beta(s)$ and $F_p(s)$ were also obtained from the PDT design.

Given the dashed tracking bounds of Fig. 5 and estimates of least upper bounds for cross-coupling from Fig. 6, the formal QFT procedure could begin. In addition to the bounds, estimates of the required QFT compensation, valid in a broad frequency range around the crossover frequencies could be obtained from Eq. 8.

Dynamic Inversion for the Formal QFT Design

The formal QFT procedure includes models of the actuators which drive the five control effectors. These models, along with the associated rate and amplitude limits are given in Table 1. The addition of the actuators requires a new dynamic inversion design. The resulting design led to a nominal effective plant matrix

$$\mathbf{P}_e(s) = \begin{bmatrix} \frac{900}{s(s+30)^2} & 0 \\ 0 & \frac{900}{s(s+30)^2} \end{bmatrix} \qquad (11)$$

As compared to the elements of Eq. 10, six, as opposed to two, poles of the effective plant $\mathbf{P}_e(s)$ can be placed with the design, i.e., $\sum_{i=1}^{2} d_i = 6$. However, the plant plus actuators and yaw-rate feedback now has 14 states. The pair of poles in each diagonal element of the effective plant at 30 rad/s are well above the crossover frequencies predicted by the PDT which means that the formal QFT design will begin with nominal loop transmissions of desirable form, i.e., approximately *1/s* in the region of crossover. Although the nominal

effective plant has now changed, the PDT is not repeated as it was intended only to serve as a prelude to the formal QFT procedure.

At this juncture it is important to point out that the elements of the dynamic inverse compensator $G_{c_p}(s)$ will involve transfer functions of order 14, i.e., the order of the effective plant. If the analyst wishes, an attempt can be made to reduce the order of these elements. This may be desirable since $G_{c_p}(s)$ will be part of the final compensator $G_{c_p}(s)G_c(s)$. Here, this simplification was undertaken after the final compensator matrix $G_{c_p}(s)G_c(s)$ was determined.

Formal QFT Design

For the sake of brevity, the details of the QFT design will not be presented here. The QFT technique, itself, has been adequately explained elsewhere, e.g., Ref. 11. The QFT design utilized the tracking performance bounds shown in Fig. 5 and cross-coupling bounds shown in Fig. 6. A relative stability requirement was introduced by enforcing a maximum amplitude ratio of 1.58 dB for all closed-loop tracking transfer functions. To put this number in context, for a second order system, this amplitude peak would correspond to 5.26 dB of gain margin and 56.44 deg of phase margin. Allowing only small amplitude peaking in any of the closed-loop tracking transfer functions contributes to the validity of the handling qualities evaluation where only the upper and lower tracking bounds are considered for evaluation.

The formal QFT procedure was completed using "Method 1", i.e., no sequential loop closure design was necessary.[11] After the design, closed-loop stability for each configuration was verified in a separate analysis. Figures 7 and 8 summarize the tracking and cross-coupling performance of the formal QFT design. The similarity between these figures and those for the PDT (Figs. 5 and 6) is noteworthy. The similarity in tracking performance would have been greater had the same prefilters been employed in the formal QFT design as in the PDT. As an example of the utility of the PDT, Fig. 9 compares the Bode diagrams for element (1,1) in $G_{c_p}(s)\cdot G_c(s)$ obtained from the PDT and the formal QFT procedure. Again, the similarity is noteworthy. Finally, the crossover frequencies associated with the β and p loops for the nominal configuration were $\omega_{c_\beta} = 3.0$ *rad/s*, $\omega_{c_p} = 7.0$ *rad/s*, respectively. These compare very favorably with the results of the PDT where values of 3.0 and 6.0 rad/s were obtained. Figure 9 also indicates that there is a significant "cost of feedback" associated with control of β. That is, element (1,1) in $G_{c_p}(s)\cdot G_c(s)$ increases in magnitude beyond crossover, and will amplify sensor noise propagated to the actuators. Similar characteristics are evident in element (1,2), not shown. This result, which was also clearly evident in the PDT, may mean that a *"beta-dot"* sensor or estimator is warranted in this application to reduce sensor noise.

It was found that simplification of the final compensator $G_{c_p}(s)\cdot G_c(s)$ was possible with little impact upon the magnitude or phase of $G_{c_p}(j\omega)\cdot G_c(j\omega)$. The elements of this final, simplified compensator are given in Table 2 along with the prefilters. Also shown are the elements of the QFT compensation matrix, alone ($G_c(s)$). Note the simplicity of the elements of the QFT compensator, alone. As mentioned in the preceding, the higher-order nature of the final compensator, even with some order reduction is attributable to the dynamic inverse. Further simplification of the elements of $G_{c_p}(s)\cdot G_c(s)$ is possible, but was not pursued here. The results of Figs. 7 and 8 do not consider the effects of possible actuator amplitude and/or rate saturation, a subject to be considered next.

Performance with Actuator Limits

Control system performance at a single flight condition was next considered where the limitations of the actuators were introduced, i.e., performance was obtained with the actuator amplitude and rate limits given in Table. 1. The flight condition was selected as Mach No. = 0.3 and altitude = 10,000 ft. This condition occurs in a corner of the Mach No. vs altitude plot of the 15 flight conditions. A nonlinear simulation was created which included the nonlinear actuator characteristics, with and without the software limiters of Fig. 1. No changes in the elements of the compensation matrix $G_c(s)\cdot G_{c_p}(s)$ were necessary other than subsuming the differentiating "s" into each compensator element and into $G_r(s)$ when the software limiters were used. No other changes were required

since examination of $\left|\frac{\beta}{n_1}(j\omega)\right|$, $\left|\frac{\beta}{n_2}(j\omega)\right|$, $\left|\frac{p}{n_1}(j\omega)\right|$, $\left|\frac{p}{n_2}(j\omega)\right|$ at frequencies below crossover indicated that the desired attenuation was occurring with no increases in system type.

Figures 10 and 11 show the vehicle roll-rate and sideslip responses to a doublet roll rate command consisting of four alternating pulses of 60 deg/s amplitude, each lasting two seconds. The responses without and with the software limiters are shown. The sideslip command was $\beta_c = 0$. Figures 12 and 13 show the output of the yaw thrust actuator without and with the software limiters. The figures indicated that both amplitude and rate limiting are occurring in this actuator. The performance improvement in the case when the software limiters are in operation is obvious. Note that, without the software limiters, the yaw thrust actuator remains in alternating states of rate saturation well beyond the time when the input command disappears. One important point to emphasize is the fact that, when the software limiters are being used, the actuator in Fig. 13 is not in hard rate saturation. It is merely following a command input that takes in up to its rate limit. It is, however, occasionally experiencing amplitude saturation.

A remaining problem involves evaluation of handling qualities and PIO susceptibility when actuator saturation is occurring, i.e., when the vehicle description involves fundamental nonlinearities. Some progress has been made in this area[18] and the issue is the subject of current research.

Conclusions

A technique for the design of robust, decoupled flight control laws for manually controlled aircraft in which actuator rate saturation occurs has been proposed. The technique has its basis in Quantitative Feedback Theory. A structural model of the human pilot is employed to provide tracking performance bounds which are predicted to yield level 1 handling qualities and no susceptibility to pilot-induced oscillations. Dynamic inversion allows the design of a precompensation matrix which approximately decouples the flight control law and creates an effective plant which is relatively easy to compensate with the Quantitative Feedback Theory procedure. A Pre-Design Technique allows the estimation of tracking and cross-coupling performance, cross-coupling bounds, nominal crossover frequencies, compensation elements and prefilters prior to invoking the formal Quantitative Feedback Theory design. Finally, a technique for improving control system performance in the presence of actuator rate saturation, previously limited to control structures where each actuator is driven by only one compensated error signal is extended to control structures in which each actuator can be driven by more than one compensated error signal. A nonlinear simulation demonstrated the utility of the software limiters in improving system performance.

Acknowledgement

This research was supported by NASA Langley Research Center under grant No. NAG1-1744. Dr. Barton Bacon was the contract technical manager.

References

[1]Hess, R. A., and Henderson, D. K., "QFT Multi-Input, Multi-Output Design with Non-Diagonal, Non-Square Compensation Matrices," Proceedings of the 13th World Congress, International Federation of Automatic Control, San Francisco, 30 June- 5 July, 1996, Vol. H, pp. 309-314.

[2]Hess, R. A., and Snell, S. A., "Flight Control System Design with Rate saturating Actuators," *Journal of Guidance, Control, and Dynamics*, Vol. 20,. No. 1, 1997, pp. 90-96.

[3]Hess, R. A., "A Unified Theory for Aircraft Handling Qualities and Adverse Aircraft-Pilot Coupling," *Journal of Guidance, Control, and Dynamics*, to appear.

[4]Snell, S. A., and Stout, P. W., "Robust Control of Angle of Attack Using Dynamic Inversion Combined with Quantitative Feedback Theory," AIAA Paper 96-3783, AIAA Guidance, Navigation and Control Conference, July 29-31, 1996, San Diego, CA.

[5]Henderson, D. K., and Hess, R. A., "Estimating Controller Performance and Cost of Feedback in MIMO QFT Designs," *Journal of Guidance, Control, and Dynamics*, to appear.

[6]Anon, "Aviation Safety and Pilot Control - Understanding and Preventing Unfavorable Pilot-Vehicle Interactions," Report of the NRC Committee on the Effects of Aircraft-Pilot Coupling on Flight Safety, National Academy Press, 1997.

[7]Adams, R. J., Buffington, J. M., Sparks, A. G., and Banda S. S., "An Introduction to Multivariable Flight Control System Design," Air Force Wright Laboratory, WL-TR-92-3110, Oct. 1992.

[8]Voulgaris, P., and Valavani, L., "High Performance Linear Quadratic and H-Infinity Designs for a Supermaneuverable Aircraft'," *Journal of Guidance, Control, and Dynamics*, Vol. 14, No. 1, 1991, pp. 157-165.

[9]Osman, C., Pachter, M., and Houpis, C. H., "Active Flexible Wing Control Using QFT," Proceedings of the 13th World Congress, International Federation of Automatic Control, San Francisco, 30 June- 5 July, 1996, Vol. H, pp.315-320.

[10]Miller, R. B., Horowitz, I. M., Houpis, C. H., and Barfield, A. F., "Multi-input, Multi-output Flight Control System Design for the YF-16 using Nonlinear QFT and Pilot Compensation," *International Journal of Robust and Nonlinear Control*, Vol. 4, No. 1, 1994, pp. 211-230.

[11]Houpis, C. H., "Quantitative Feedback Theory (QFT) for the Engineer, A Paradigm for the Design of Control Systems for Uncertain Nonlinear Plants," Flight Dynamics Directorate, Wright Lab., WL-TR-95-3061, June 1995.

[12]Horowitz, I., "Survey of Quantitative Feedback Theory," *International Journal of Control*, Vol. 53, No. 2, 1991, pp. 255-291.

[13]Catapang, D. R., Tischler, M. B., and Biezad, D. J., "Robust Crossfeed Design for Hovering Rotorcraft," *International Journal of Robust and Nonlinear Control*, Vol. 4, No. 1, 1994, 161-180.

[14]Yaniv, O., "MIMO QFT Using Non-Diagonal Controllers," *International Journal of Control*, Vol. 61, No. 1, 1995, pp. 245-253.

[15]Enns, D., Bugajski, D., Hendrick, R., and Stein, G., "Dynamic Inversion: An Evolving Methodology For Flight Control," *International Journal of Control*, Vol 59, No. 1, 1994 pp. 71-91.

[16]Snell, S. A., Enns, D. F. and Garrard, W. L., "Nonlinear Inversion Flight Control for a Supermaneuverable Aircraft," *Journal of Guidance, Control, and Dynamics*, Vol. 15, No. 3, 1992, pp. 976-984.

[17]Klyde, D. J., McRuer, D. T., and Myers, T. T., "Pilot-Induced Oscillation Analysis and Prediction with Actuator Rate Limiting," *Journal of Guidance, Control, and Dynamics*, Vol. 20, No. 1, 1997, pp. 81-89.

[18]Hess, R. A., and Stout, P. W., "Assessing Aircraft Susceptibility to Nonlinear Aircraft-Pilot Coupling/Pilot-Induced Oscillations," AIAA Paper No. 97-3496, 1997 AIAA Atmospheric Flight Mechanics Conference, New Orleans, LA, Aug. 11-13, 1997.

Table 1. Actuation and Control Distribution Characteristics

control effectors

δ_{DT} = differential horizontal stabilizer, deg
δ_A = aileron, deg
δ_R = rudder, deg
δ_{RTV} = differential pitch thrust vectoring, deg
δ_{YTV} = yaw thrust vectoring, deg

control distribution matrix, K

$$K = \begin{bmatrix} 0 & 0 & 100 & 0 & 60 \\ 60 & 100 & 0 & 60 & 0 \end{bmatrix}^T$$

Actuator Dynamics[a]:

δ_{DT}:	$\frac{30^2}{[.707,30]}$	rate limit = 60 deg/s	ampl. limit = ± 17.5 deg
δ_A:	$\frac{75^2}{[.59,75]}$	rate limit = 100 deg/s	ampl. limit = ± 27.5 deg
δ_R:	$\frac{72^2}{[.69,72]}$	rate limit = 100 deg/s	ampl. limit = ± 30.0 deg
δ_{RTV}/δ_{TV}:	$\frac{20^2}{[.6,20]}$	rate limit = 60 deg/s	ampl. limit = ± 30.0 deg

[a] $\frac{K(z_1)}{(p_1)[\zeta_1,\omega_1]} = \frac{K(s+z_1)}{(s+p_1)[s^2+2\zeta_1\omega_1 s+\omega_1^2]}$

Table 2. Compensators and Prefilters

Elements of $G_c(s)$-$G_c(s)$

$$1,1 - \frac{1.46\cdot10^4[1,.3][.792,.922](4.64)[.585,19.3](20)[.688,69.8]}{(0)^2(1)^2[.551,22.64][1,29.9](54.8)(97.6)(101.7)}$$

$$1,2 - \frac{77.3(.5)(.654)(5.23)[.586,19.3](20)[.693,69.7](-173)}{(0)^2(1)[.551,22.6](30)(54.6)(95.1)[1,102]}$$

$$2,1 - \frac{-1003(.3)^2(3.04)(-3.34)[.6,20](20)[.707,30][.59,75.0]}{(0)^2(1)[.55,22.6][1,30][.642,35.8](54.4)[1,99.8]}$$

$$2,2 - \frac{183.2(.5)(1.65)(20)[.707,30](61.9)[.59,75]}{(0)^2(30)[.641,35.8](54.4)[1,98](103.4)}$$

Elements of $G_c(s)$

$$1,1 - \frac{1666.6(.3)^2(20)}{(0)(1)(100)^2}$$

$$1,2 - 0$$

$$2,1 - 0$$

$$2,2 - \frac{2.22\cdot10^4(.5)(20)(30)}{(0)(100)^3}$$

Prefilters

$$F_\beta = \frac{0.12(100)}{(3)(4)}$$

$$F_\rho = \frac{1000}{(20)(50)}$$

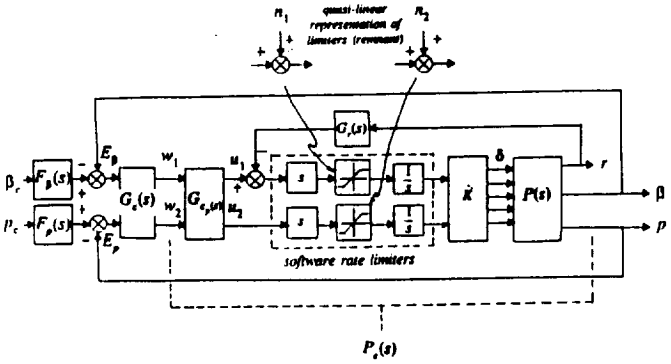

Fig. 1 The flight control system structure.

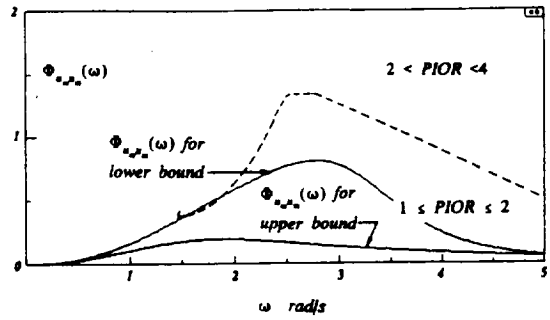

Fig. 4 Pilot-induced oscillation bounds for $\Phi_{u_m u_m}(\omega)$.

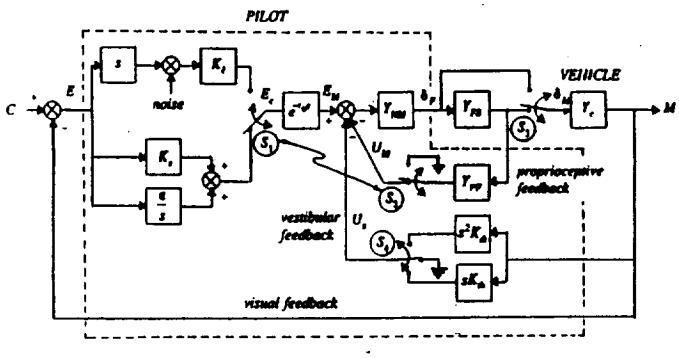

Fig. 2 A structural model of the human pilot.

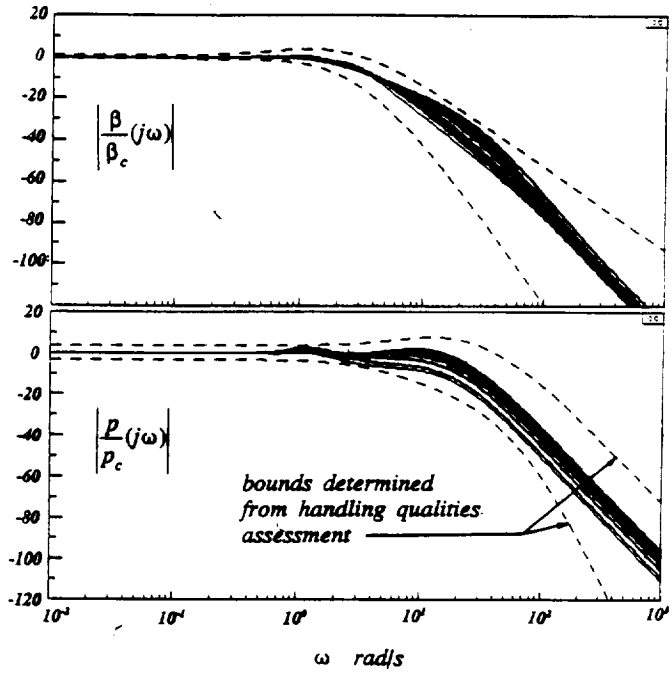

Fig. 5 Tracking performance from the PDT for fifteen flight conditions.

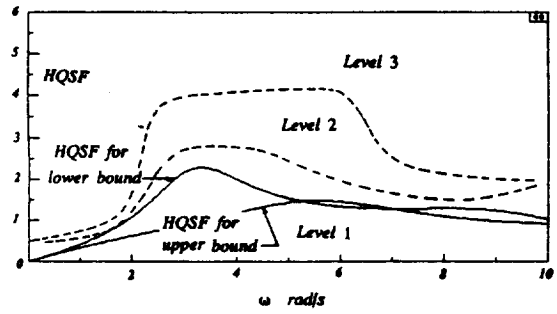

Fig. 3 Handling qualities boundaries for HQSF's

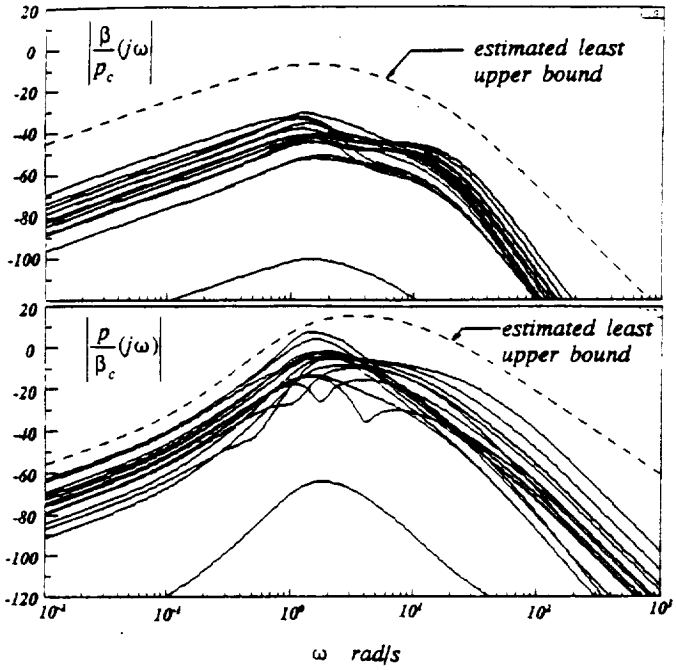

Fig. 6 Cross-coupling performance from the PDT for fifteen flight conditions.

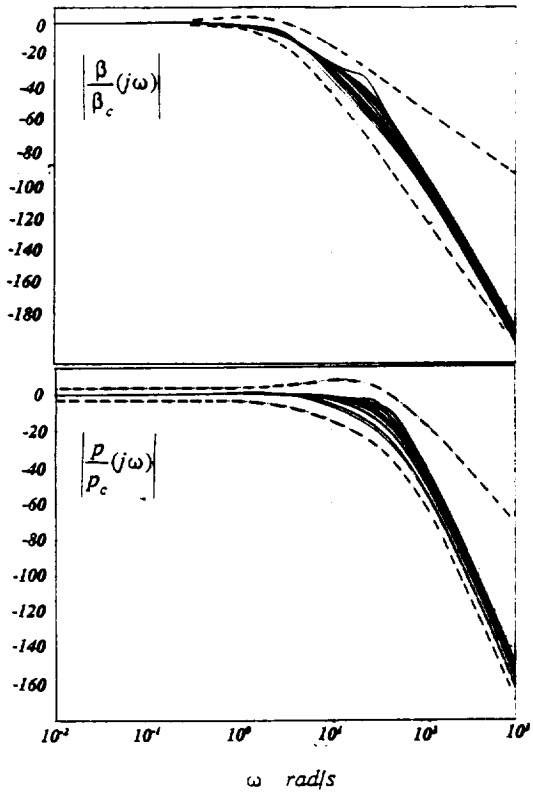

Fig. 7 Tracking Performance from formal QFT design for fifteen flight conditions.

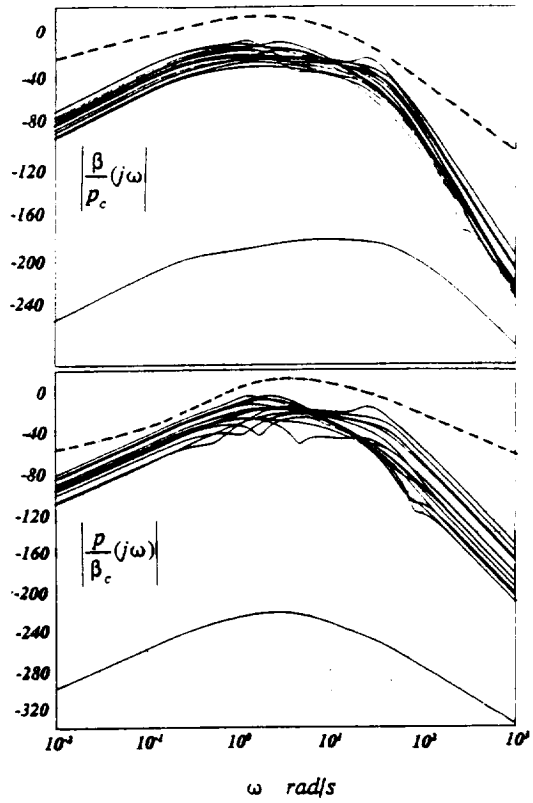

Fig. 8 Cross-coupling performance from the formal QFT design for fifteen flight conditions.

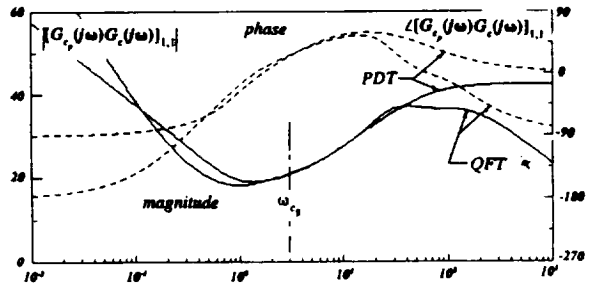

Fig. 9 Comparison of element (1,1 of $G_{c_p}(j\omega)G_c(j\omega)$ from PDT and formal QFT designs.

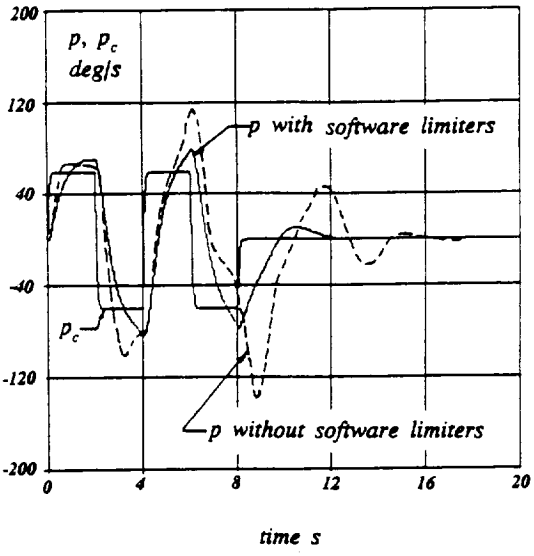

Fig. 10 Roll-rate responses to doublet roll-rate command, without and with software rate limiters.

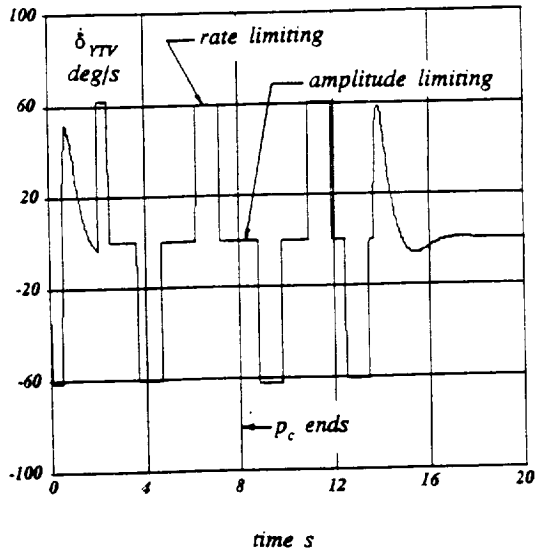

Fig. 12 Output of yaw thrust actuator without software rate limiters.

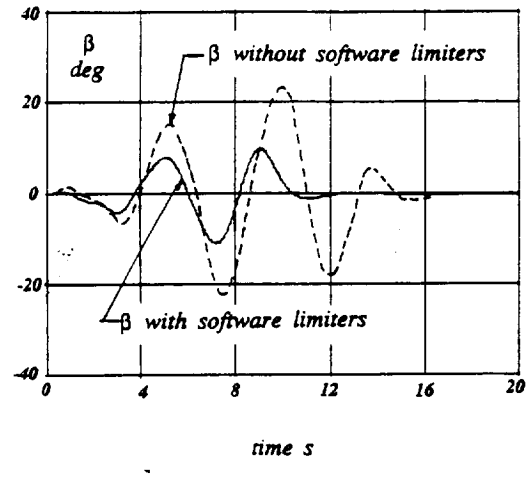

Fig. 11 Sideslip responses to doublet roll-rate command, without and with software rate limiters.

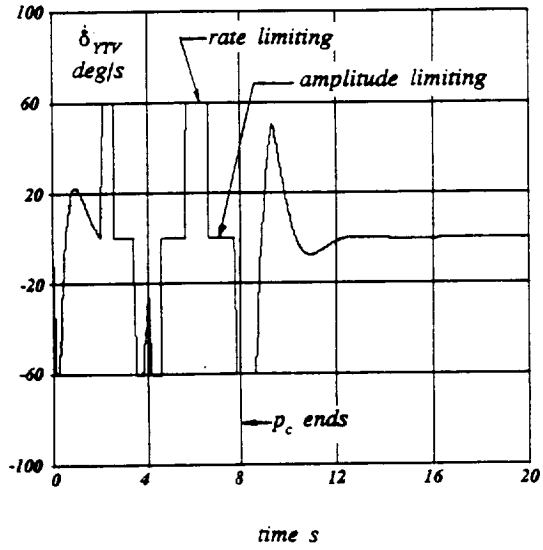

Fig. 13 Output of yaw thrust actuator with software rate limiters.